Nanocone Decorated ZnO Microspheres Exposing the (0001) Plane and Enhanced Photocatalytic Properties

Dr. Heather F. Greer,[†#]* Prof. Wuzong Zhou,[†] Dr. Guan Zhang,[†] and Dr. Hervé Ménard[‡]

[†] EaStChem, School of Chemistry, University of St Andrews, Fife KY16 9ST, United Kingdom
E-mail: hfg24@cam.ac.uk
[‡] Sasol Technology (UK) Ltd, Purdie Building, North Haugh, St Andrews, Scotland KY16 9ST, United Kingdom
[#]Current address: Department of Chemistry, University of Cambridge, Lensfield Road, Cambridge CB2 1EW

ZnO spherical particles exposing only the (0001) planes were prepared by an established solvothermal method using a water–ethylene glycol (EG) mix as a solvent. It was found that poorly crystalline nanoparticles formed first, followed by their aggregation into microspheres consisting of crystallites embedded in ethylene glycol and precursor molecules/ions. The grown up nanocrystallites and nanocones in the microspheres are all radially aligned. The possible formation mechanisms, in particular, the roles of water molecules, ethylene glycol and the intrinsic dipolar field of ZnO crystals, are discussed. X-ray photoelecton spectroscopy (XPS) experiments indicated the spherical particles were terminated solely by zinc atoms. Brunauer-Emmett-Teller (BET) measurements in conjunction with the degradation of methylene blue (MB) dye data demonstrated that the photocatalytic performance of the ZnO spheres depended on the growth time and was significantly improved compared to traditional ZnO nanorods. This study is a rare example which combines nanostructural characterisation of ZnO particles terminated with a single (0001) plane of known Zn^{2+}-polarity with their photocatalytic performance.

1. Introduction

Zinc Oxide is an important semiconductor, with a wide band-gap (3.37 eV) and a large exciton binding energy (60 meV). The distinct optical and electronic properties combined with the huge morphological variety makes ZnO a promising candidate material for applications in catalysis,[1] dye-sensitized solar cells[2] and light emitting diodes,[3] etc. Desired chemo-physical properties related to the size, shape and exposed facets of ZnO have led to many novel morphologies including nanotubes,[4] nanonails,[5] flowers,[6] rings[7], tetrapods[8] core-shell microspheres[9], and hierarchical nanostructures composed from rod[10,11] and plate components.[12,13] The properties of ZnO are very sensitive to surface and core defects and therefore their defect structure is often studied on the atomic scale using electron paramagnetic resonance (EPR) and photoluminescence (PL) spectroscopy.[14]

The growth habit and therefore the morphology of ZnO is governed by the three most common crystal faces, $\{10\bar{1}0\}$, $\{11\bar{2}0\}$ and $\{0001\}$. The $(10\bar{1}0)$ surfaces are the most stable, whilst the $\{0001\}$ surfaces exhibit the highest surface energy of the low-index planes and usually grow too fast to be observed in the final morphology.[15] This can explain the frequent observation of ZnO rods, where, anisotropic crystal growth along the c-axis maximises the area of the non-polar $\{10\bar{1}0\}$ surfaces and minimises the polar $\{0001\}$ surfaces. Surfactants or capping agents can be added to reduce the surface energy of the $\{0001\}$ polar and $(10\bar{1}1)$ semi-polar facets, and slow down their growth rate. Therefore these planes can appear as exposed surfaces in the form of novel morphologies such as hexagonal nanopyramids and nanocones.[16-18] The wurtzite crystal structure of ZnO shows spontaneous electrical polarization along its c-axis.[15] The positive polar face (0001), termed the c(+)-plane is rich in zinc atoms whilst the negative polar face $(000\bar{1})$, termed the c(-)-plane is rich in oxygen atoms.

The chemical stability and photocatalytic activity of ZnO strongly depend on the specific exposed planes and their polarity. By varying the ethylene glycol-H_2O volume fraction, Huang et al.[19] were able to prepare three different morphologies of ZnO with different

exposed facets. This adjusted the exposed facets from nonpolar $\{10\bar{1}0\}$ and polar $\{0001\}$ planes in a hexagonal prism, to semi-polar $\{10\bar{1}1\}$ and polar $\{0001\}$ planes in a hexagonal bifrustum, and finally to polar $\{0001\}$ planes in ZnO spheres. The photo degradation efficiencies for the different surfaces of ZnO as estimated by degradation of Rhodamine B (RhB) dye was proven as $\{0001\} > \{10\bar{1}1\} > \{10\bar{1}0\}$. Therefore, ZnO morphologies exposing only c-planes or predominately c-planes can be expected to exhibit better photocatalytic behaviour.

Very few examples of ZnO particles exposing only c-planes have been reported, of which even fewer have had their properties investigated.[20-23] Matsumoto et al.[22] prepared ZnO microspheres consisting of wedge nanocrystallites radially aligned along the c-axis in a mixed ethylene glycol-H_2O solvent. Convergent beam electron diffraction (CBED), known to give reliable data on the polarity of ZnO nanomaterials, confirmed that only the c(+)-plane, *i.e.* the positively terminated face of the (0001) plane, was exposed. This was thought to be the first time polycrystalline particles exposing only one specific crystal plane and with known polarity were reported. Saito et al.[23] discovered that these ZnO spherical particles worked well as a volatile organic compounds (VOC) gas sensor, with the best sensitivity obtained for ethanol. Li et al.[20] found that a series of ZnO morphologies including prisms, dumbbells and twin-spheres exposed in ±(0001) facets can be achieved by adjusting the molar ratio of sodium bis(2-ethylhexyl) sulfosuccinate (AOT) to Zn^{2+} from 8.1 to 0.5: 1. A stepwise self-assembly mechanism was proposed to understand the formation of these twin-spheres, whose growth begins with 1D prisms which not only act as a seed but also as a bridge to connect the two hemispheres of the twin-spheres together. Strong and anisotropic blue emission at the central area of the ZnO twin-spheres attributed to their special topological surfaces terminated by ±(0001) planes suggests that novel devices could be fabricated if the microstructure is carefully tailored. Additionally, ZnO hollow spheres with surface exposed c-planes are

expected to outperform ZnO solid microspheres by possessing additional potential in gas sensing, drug delivery and microcapsule reactors.[21,24] Other transition metal oxides prepared with their highly reactive {001} facets preferentially exposed include TiO_2 [25] and CuO,[26] which offer superior photocatalytic, electrochemical and gas sensing performances.

Alongside the exposed planes, polarity is also an important point to consider when preparing ZnO materials. Gautam et al.[27] prepared two distinctive concentric assemblies of ZnO rods, where the rods emanate out of a central core and maintain a single polar direction. Scanning electron microscopy (SEM) and transmission electron microscopy (TEM) images showed the assemblies terminate with a tip of varying morphology and angular orientation, either smooth (yield 70–80 %) or sharp, pencil-like. Comparison of experimental and simulated CBED patterns unambiguously confirmed the smooth tips grow along the O-polar direction, whereas the sharp tips grow along the Zn-polar direction. Strong UV luminescence was exhibited in the exterior of the Zn-polar assemblies, unlike the O-polar assemblies. The Zn-terminated (0001) surface of ZnO has often been reported to be much more catalytically active than the O-terminated (000$\bar{1}$) polar surface which is said to be inert in comparison.[22] This is consistant with the work of Misha et al.[8] where ZnO tetrapod with different nanoarm morphologies displayed varying photocatalytic decolourisation rates.

In the present work, the time-dependent crystal growth of nanotile decorated ZnO spherical polycrystalline particles terminated by *c*-planes was investigated. These ZnO specimens contain radially aligned nanocrystallites or nanocones. Specimens were predominately characterised by powder X-ray diffraction (XRD) and electron microscopy techniques. A new formation mechanism is proposed. The time-dependent photocatalytic performance of the ZnO specimens was studied through the degradation of MB dye. It is expected that this simple but controllable solvothermal synthetic method can further inspire the preparation of other metal oxides with exposed highly active surfaces with a focus on refining their properties according to their morphology at a given reaction time.

2. Results and Discussion

ZnO particles obtained after a reaction time of 48 h at 95 °C in 85% and 95%-EG solutions have a highly uniform spherical morphology as shown by the SEM images in **Figure 1(a,b)**. The size of the spherical particles prepared in 85%-EG are in a range of 5.5 − 11.8 µm, whilst the ZnO particles prepared in 95%-EG are much smaller, being varied between 3.1 and 5.2 µm in diameter. Higher magnification SEM images as shown in **Figure 1(c-f)** confirm the surface of both varieties of ZnO spherical particles are covered in nanotiles. In the particles
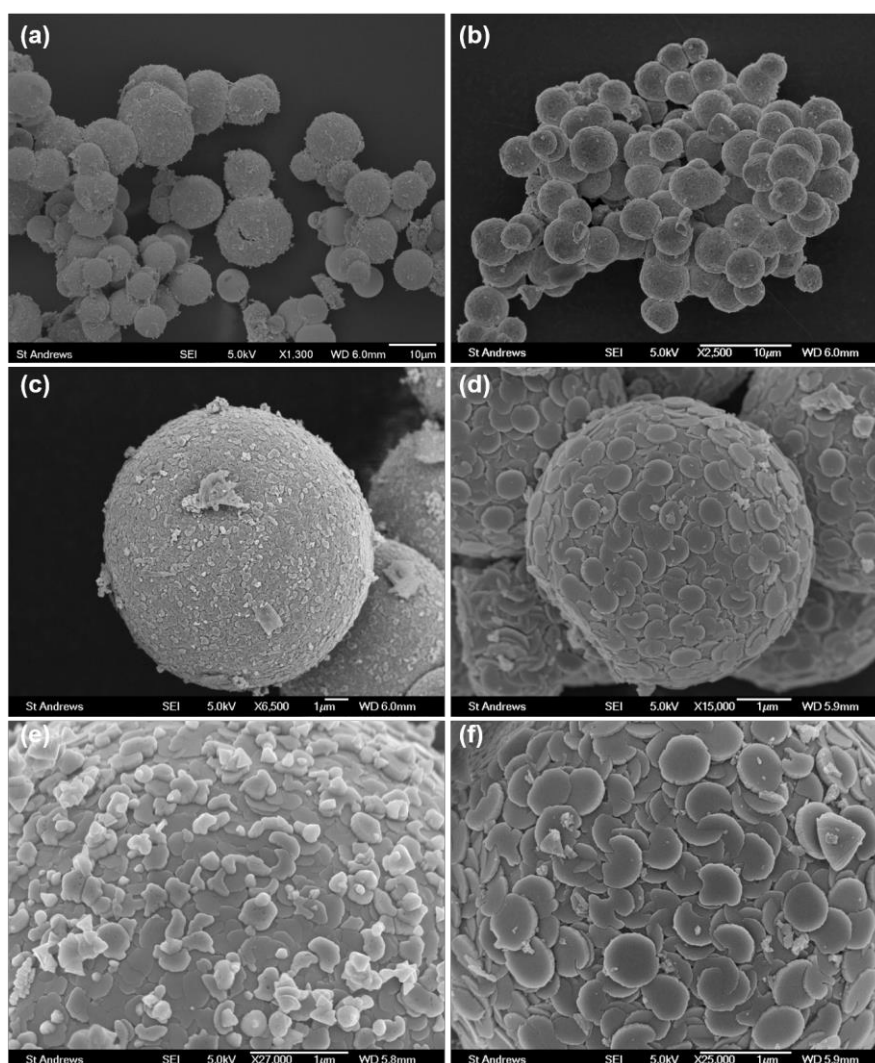

Figure 1. SEM images with different magnifications of ZnO particles prepared under solvothermal conditions for 48 h in (a,c,e) 85%-EG and (b,d,f) 95%-EG.

prepared in 85%-EG, the nanotiles are irregular shaped with a dimension of 200–400 nm (**Figure 1e**), whilst the tiles are circular with a dimension of 400–600 nm on the particles

prepared in 95%-EG (**Figure 1f**). Similar particles were previously produced by Matsumoto, et al.,[22] and it was suspected that EG played an important role in the formation of these morphologies. However, we believe that the role of water molecules is even more crucial, since they are directly involved in the crystal growth of ZnO. Another essential condition is zinc acetate dihydrate as the precursor compound. When $Zn(NO_3)_2.6H_2O$ was used to replace $Zn(O_2CCH_3)_2.2H_2O$, nanoparticles, ca. 30–40 nm in diameter, were obtained without the morphologies shown in **Figure 1** (**ESI,† Figure S1**). To understand the evolution of the internal structures and step-by-step crystal growth of the nanotile decorated ZnO spherical particles, specimens with different reaction times were prepared.

2.1. ZnO prepared in 95%-EG

Little structural information and testing of the properties of the time dependent ZnO specimens prepared in 95%-EG at 95 °C has been done in literature. The shortest reaction time we used in this work was 10 h, when a sufficient amount of precipitate could be collected. The product contained 60 - 90 nm sized nanoparticles (**Figure 2a**), which further aggregated into large spheres, 1.4 – 4.5 μm in diameter with a very rough surface (**Figure 2b**).

High resolution transmission electron microcopy (HRTEM) images (**Figure 2c**) show the precipitate has a very low crystallinity and that unoriented ZnO nanocrystallites are embedded in an amorphous matrix. The high amorphous content visualised during TEM characterisation is likely related to the 6.9 wt% EG detected from thermal gravametric analysis (TGA) of the 10 h specimen (**ESI,† Figure S2**). Energy dispersive X-ray spectroscopy (EDX) results indicate that the particles contain mainly Zn and O with a small amount of C. The average atomic ratio of C : O : Zn is about 10 : 50 : 40 (**Figure 2d**). Consequently, the spherical particles are initially aggregates of precursor molecules, due to relatively strong interaction between these molecules, such as $Zn(O_2CCH_3)_2·2H_2O$, EG and H_2O, etc. Polymerisation of zinc acetate would be a key step of the aggregation. Considering the low dissociation constant

of zinc acetate dihydrate, the concentration of Zn^{2+} and O^{2-} would be extremely low in the synthetic solution. The nucleation and growth of ZnO crystals from zinc acetate can only be achieved by a hydrolysis process. The intermediate states of this process are polymerised zinc acetate.
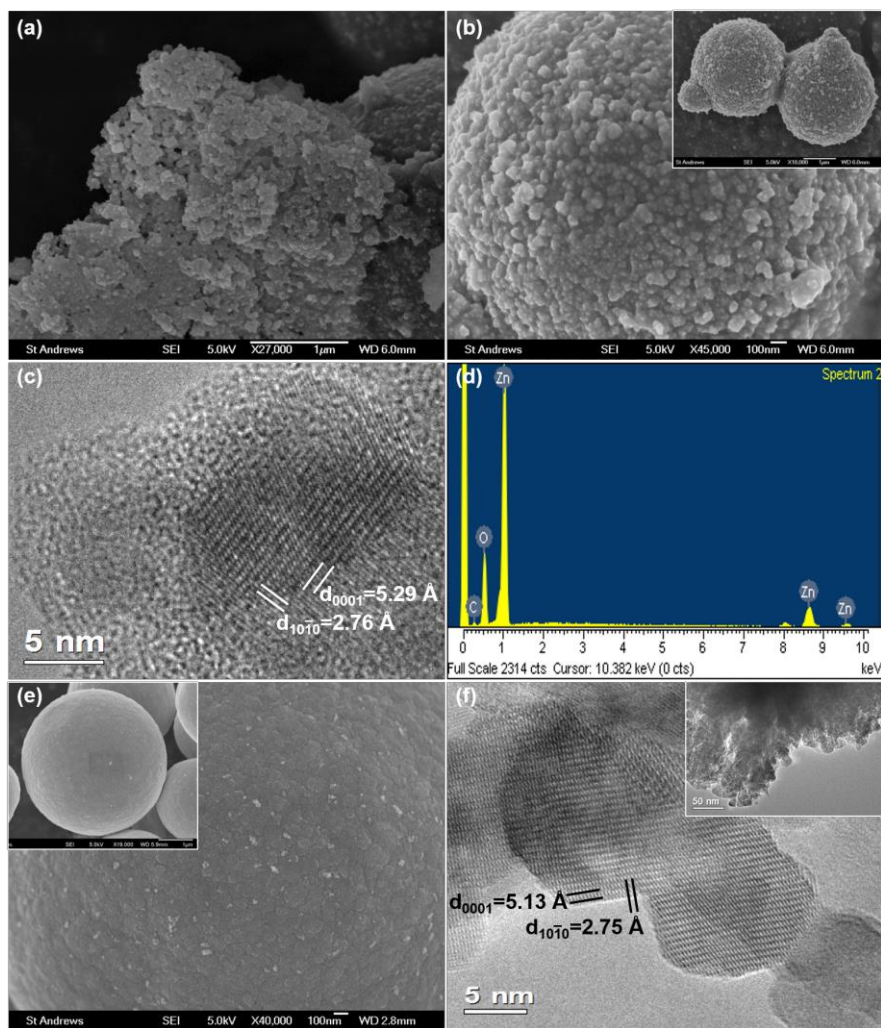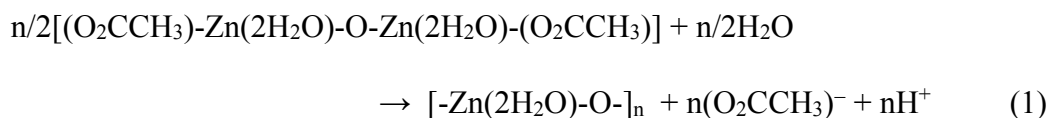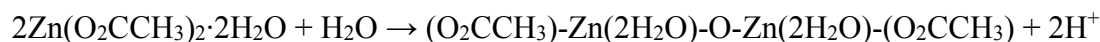

Figure 2. Electron microscopic images recorded from ZnO particles prepared in 95%-EG for a reaction time of (a-d) 10 h and (e,f) 12 h. (a) SEM image of irregular shaped aggregates of nanoparticles. (b) High magnification SEM image of the rough surface of a spherical particle. A low magnification SEM image is shown in the inset. (c) HRTEM image showing nanocrystallites embedded in an amorphous matrix. (d) EDX spectrum showing peaks from C, O, and Zn. (e) High magnification SEM image of a spherical particle displaying a higher density and a smoother surface. A low magnification SEM image in shown in the inset. (f) HRTEM image of oriented nanoparticles in a microsphere. A low magnification TEM image is shown in the inset.

Zn^{2+} cations are normally tetrahedrally or octahedrally coordinated. In the molecular crystals of $Zn(O_2CCH_3)_2 \cdot 2H_2O$, Zn^{2+} are 6 coordinated,[28] which can be maintained when it is

7

dissolved in the EG/water solvent and later in the aggregates. The zinc acetate molecules then polymerised in a hydrolysis process into a dimer and then a polymer as shown by **Equation (1)**.

$$2Zn(O_2CCH_3)_2 \cdot 2H_2O + H_2O \rightarrow (O_2CCH_3)\text{-}Zn(2H_2O)\text{-}O\text{-}Zn(2H_2O)\text{-}(O_2CCH_3) + 2H^+$$

$$n/2[(O_2CCH_3)\text{-}Zn(2H_2O)\text{-}O\text{-}Zn(2H_2O)\text{-}(O_2CCH_3)] + n/2H_2O$$

$$\rightarrow [\text{-}Zn(2H_2O)\text{-}O\text{-}]_n + n(O_2CCH_3)^- + nH^+ \qquad (1)$$

The polymer finally dehydrated and re-arranged into crystalline ZnO.

The increase of the acidity from the above reaction can be neutralised by hexamethylenetetramine (HMT). Due to the low concentration of water, the crystal growth is very slow. The experimental observations in the present work indicate that nucleation of ZnO takes place inside the aggregated spherical particles rather than in the solution. Furthermore, affected by slow diffusion of water molecules into the particles, we can expect that the most active crystal growth sites to be on the surface of the spheres, this having been confirmed in our examination of the later samples.

An aggregation step has been commonly observed during investigations of the early growth stages of materials following the reversed crystal growth route.[29,30] In those systems, large organic molecules were introduced into traditional synthetic methods, strengthening the interaction between molecules or small particles, leading to the formation of disordered spherical particles. During extended hydrothermal treatment, re-crystallization takes place on the particle surface to form a thin monocrystalline polyhedral shell, followed by re-crystallisation from the surface to the core, gradually approaching to a single crystal state. However, the synthetic system in the present work did not lead to any single-crystalline polyhedral shells.

When the reaction time in the present work was extended to 12 h, the surface of the spherical particles became much smoother and their density increased (**Figure 2e**). Reduction

in the surface roughness accompanied by an increase in density would have reduced the surface free energy to make this morphology more thermodynamically stable.

The XRD pattern of the 12 h sample can be indexed to a pure phase of hexagonal wurtzite ZnO (JCPDS card no. 70-2551) with unit cell parameters of a = 3.249, c = 5.207 Å, space group P63mc (**Figure 3a**). The average crystallite size was calculated to be about 26 nm in diameter using the Scherrer equation on the ($10\bar{1}0$), (0002) and ($10\bar{1}1$) diffraction peaks. Consequently, these spheres are still composed of many small nanocrystallites which are now oriented (**Figure 2f**).
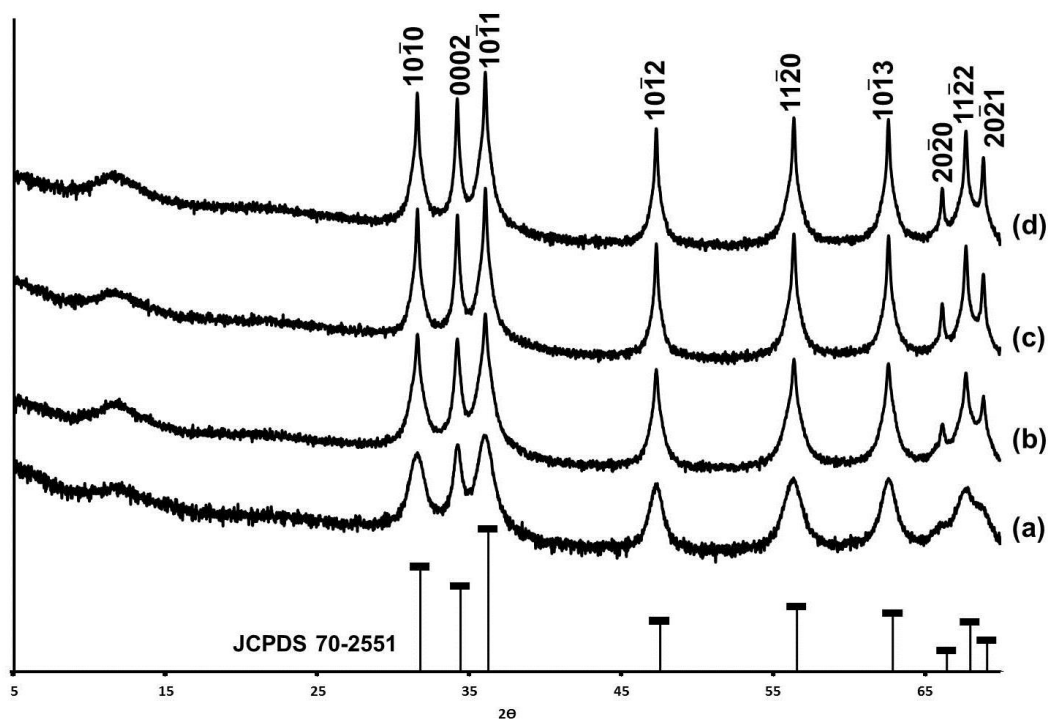

Figure 3. XRD pattern of specimens prepared in 95%-EG with a reaction time of (a) 12 h, (b) 24 h, (c) 48 h, and (d) 96 h. Pattern (d) is indexed to wurtzite ZnO. The JCPDS card for ZnO is shown for comparison.

Further increasing the reaction time to 24 h, 48 h and 96 h caused the corresponding XRD patterns to show much sharper diffraction peaks and higher intensities. The average crystal size increased significantly, e.g. 80 nm at 24 h and 129 nm at 48 h, respectively (**Figure 3b,c**).

SEM images of these samples revealed that the surface of the spheres underwent re-crystallization into nanodiscs. In our previous work, amorphous cylindrical clusters formed in an aqueous solution containing sodium citrate, zinc nitrate and HMT. Surface re-crystallization resulted in a hexagonal prism single-crystal shell.[31] In the present work, surface re-crystallization led to formation of many discs, first with random orientations as seen in the SEM images of the 18 h sample (**Figure 4a,b**), and later with all the discs lying down on the surface as shown in the SEM images of the 24 h sample (**Figure 4c,d**).

It is also noticed that the size of the discs did not increase much from 18 h to 24 h. However, the crystallinity increased significantly, indicating that the formation of the
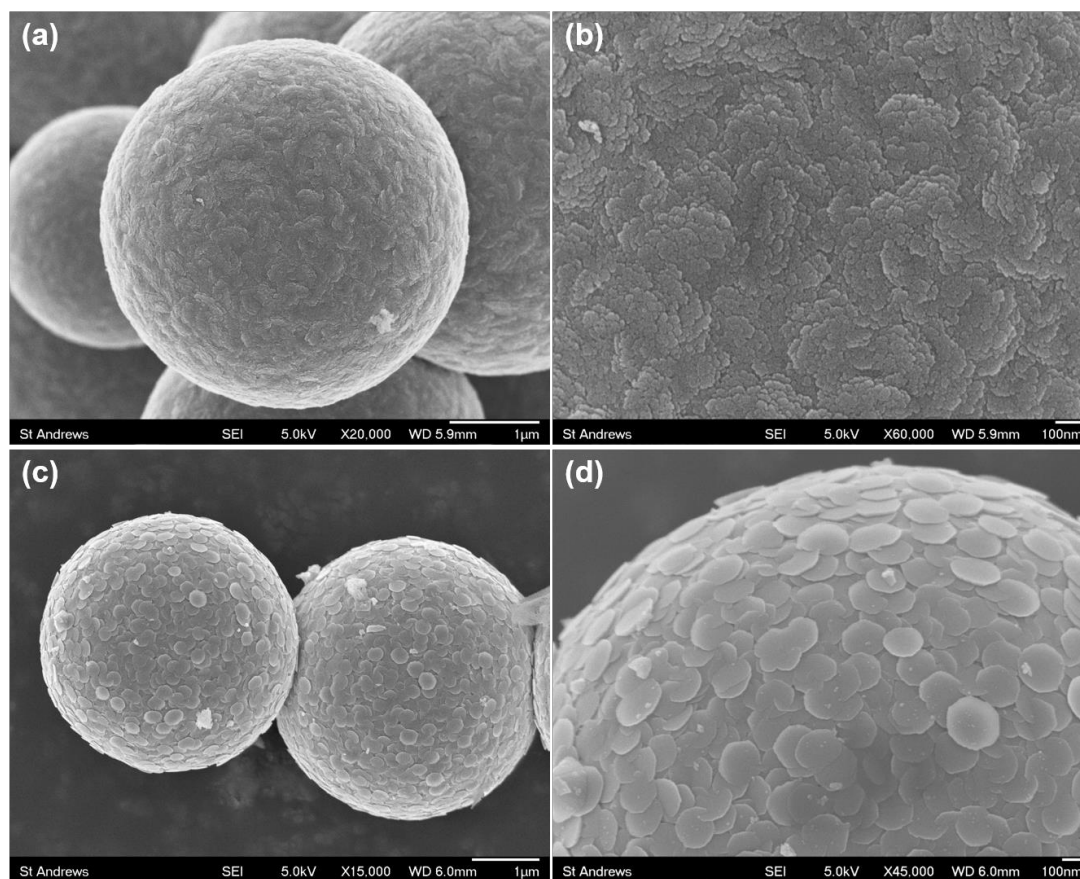

Figure 4. SEM images recorded from ZnO particles prepared in 95%-EG for a reaction time of (a,b) 18 h and (c,d) 24 h. (a,c) Low and (b,d) high magnification SEM images of spherical particles displaying different surface topologies. The particle in (a,b) has a distinctly rough surface whilst the particles in (c,d) contains surface tiles lying parallel to the surface.

nanodiscs relied on the assembly of nanocrystallites or Ostwald ripening rather than the development from a single nucleus. The formation of round discs (190-280 nm in diameter) rather than hexagonal plates or a single-crystal shell can be attributed to the surface adsorption of organic ligands, such as EG. In other words, the crystal growth along the $<10\bar{1}0>$ and $<11\bar{2}0>$ were greatly suppressed by EG molecules. In the 48 h sample, there is approximately 2.1 wt% EG as detected by TGA (**ESI,† Figure S2**). The formation of nanodiscs was not observed in the crystal growth of ZnO in an aqueous system.

The TEM image in **Figure 5a** shows a single surface nanotile and its corresponding selected area electron diffraction (SAED) pattern with a view direction of [0001]. This is evidence to show that the exposed surface of the nanotile is the (0001) plane. The HRTEM image in **Figure 5b** was recorded from the marked region in **Figure 5a**. A non-uniform contrast and the presence of many point defects are detected in this image. Further evidence of the growth direction of the surface tiles, and termination of the particles by a single crystal plane was obtained by recording HRTEM images and SAED patterns from multiple regions on a single particle (**ESI,† Figure S3**).

Further crystal growth of the discs was mainly inwards to form a surface layer of nanocones. **Figure 5c** shows the surface of a nanotile decorated sphere with one nanotile removed. The hole implies that the original nanotile has a shape of cone with the apex pointing towards the centre of the sphere. A SEM image of a half spherical particle reveals the microstructure of the cross section of a sphere in the 48 h sample is a layer of nanocones on the surface of a radial core of smaller nanocrystallites. The thickness of this layer is approximately 530 nm (**Figure 5d**), while the thickness of the surface nanocones in the 24 h sample is about 350 nm (**ESI,† Figure S4**).
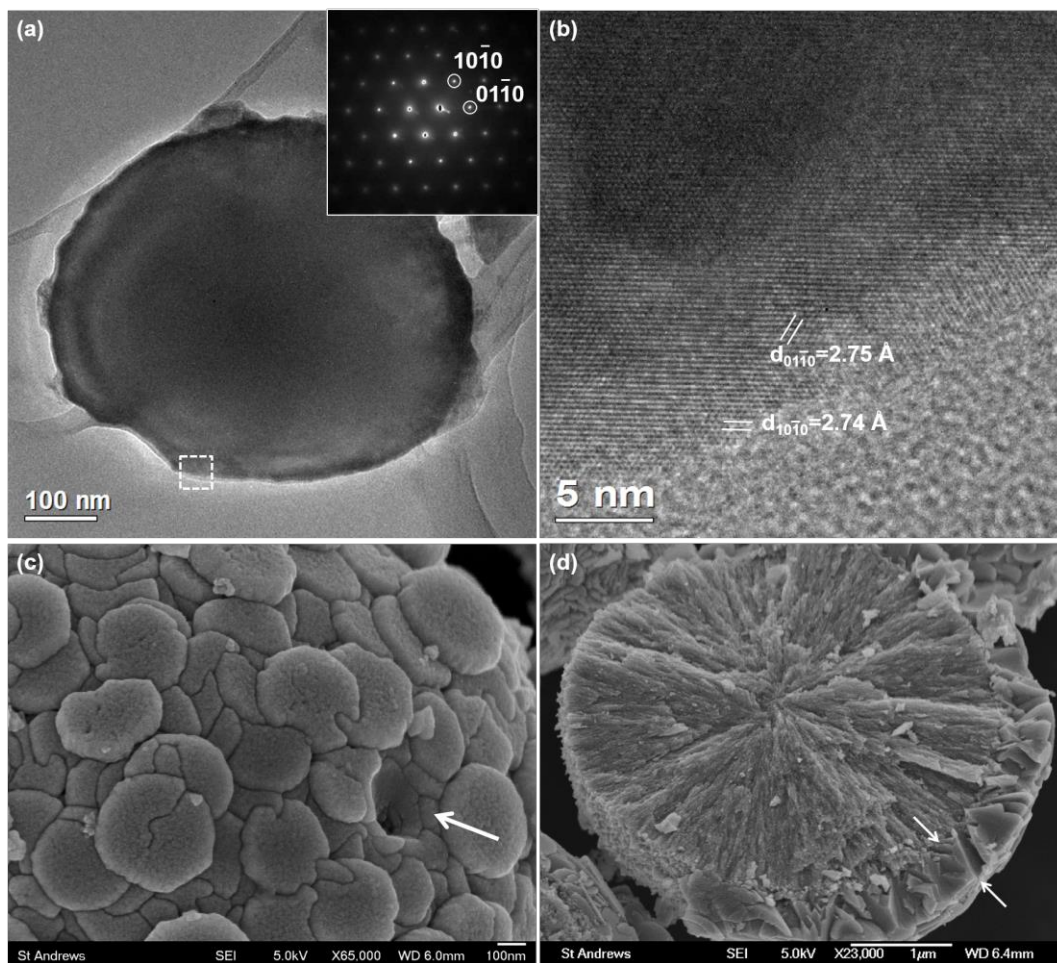
Figure 5. Electron microscopic images of particles prepared in 95%-EG with a reaction time of (a,b,d) 48 h and (c) 96 h. (a) TEM image of a single nanodisc with the corresponding SAED pattern shown in the inset, which is indexed to wurtzite ZnO. (b) HRTEM image recorded from the marked edge of the nanodisc in (a). The marked lattice fringes can be indexed to the $(10\bar{1}0)$ and $(01\bar{1}0)$ planes of ZnO. (c) High resolution SEM image of the surface of a nanotiled spherical particle, showing a cavity (marked by arrow) caused by removal of a surface nanotile. (d) SEM image of fractured ZnO particle. The arrows indicate the thickness of the tiled surface layer.

It is interesting to see that the nanocones did not develop in the core, where traces of a radial pattern appeared (**Figure 5d**). TEM and SAED were carried out on some fragments of the core region of the 24 h sample (**ESI,† Figure S5a**). The corresponding SAED pattern (inset of **ESI,† Figure S5a**) shows an ordering of the nanocrystallites. The diffusion of the diffraction spots indicates that the ordering is not perfect. A HRTEM image recorded from the same region shows partial ordering of 3 – 7 nm sized domains (**ESI,† Figure S5b**). The marked lattice fringes from two different domains have a small angle of lattice dismatching. If

these nanocrystallites line up radially, the radial pattern in the core of spheres shown in **Figure 5d** becomes understandable. This property becomes more obvious in the spherical particles formed in the 85%-EG system of which, the driving force for the ordering is discussed below.

2.2. ZnO prepared in 85%-EG

Increasing the water concentration in the solvent from 5% to 15% made a remarkable change to the speed of both the early stage aggregation and the crystal growth. The 6 h and 8 h spherical particles (**Figure 6**) have a similar size and morphology to those of the 12 h sample in the 95%-EG system (**Figure 2e**). Nanorods arranged in a spherulite manner were observed when a 6 h spherical particle was fractured (**Figure 6b**). The HRTEM image in **Figure 6c** shows a well oriented domain structure of 4 − 8 nm sized nanocrystallites with their c-axes parallel to the long axes of the nanorod. Many randomly located nano-sized non-crystalline regions, marked by arrows in **Figure 6c** are thought to be associated with the inclusion of ethylene glycol or pores which are typical in spherulite type structures.

The XRD pattern of a specimen prepared with a reaction time of 12 h (**ESI,† Figure S6a**) is monophasic and can be indexed to hexagonal ZnO. The sharpness and intensity of the reflections are much higher than that from the 12 h sample prepared in 95%-EG shown in **Figure 3a**. When the solvothermal treatment time was extended from 24 h to 96 h, wurtzite ZnO was maintained as the dominant crystalline phase although several low intensity reflections corresponding to an impurity phase appeared in the low 2Θ region (**ESI,† Figure S6b-d,7**). This impurity does not affect our elucidation of the formation mechanism of ZnO and a relevant discussion is given in **ESI†**.
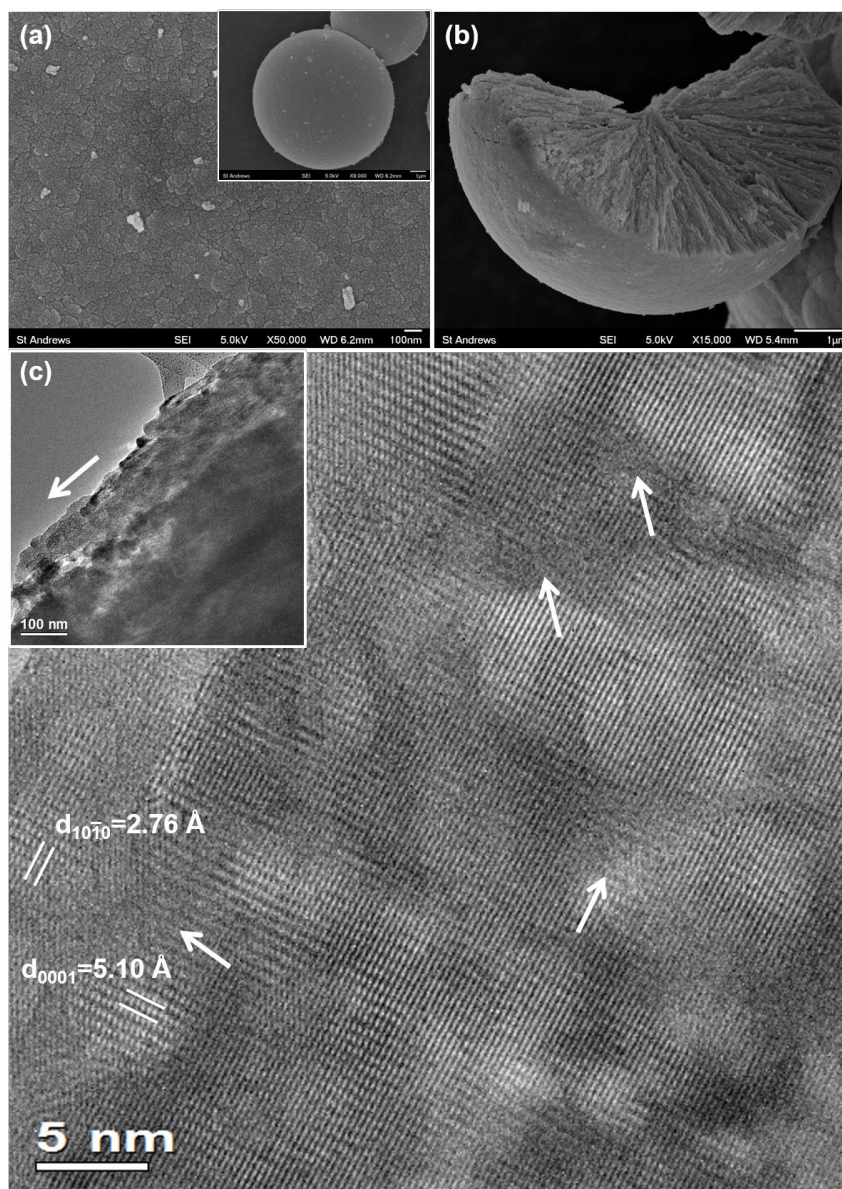
Figure 6. Electron microscopic images recorded from particles prepared in 85%-EG and with a reaction time of (a,c) 8 h and (b) 6 h. (a) High resolution SEM image recorded from the surface of a typical spherical particle from the 8 h specimen. A low magnification SEM image is shown in the inset. (b) SEM image of a fractured spherical particle showing an internal spherulite structure. (c) HRTEM image of a fragment of an inner nanorod, showing well orientated crystallites. The arrows mark pale contrasted voids. A low magnification TEM image is shown in the inset, in which the arrow points the long axis of the nanorod.

SEM images of the 10 h sample (**ESI,† Figure S8**) confirmed that the particle size is similar to that observed in the 48 h specimen (**Figure 1a**). Higher magnification SEM images (**ESI,† Figure S8b**) detected many thin nanotiles with diameters of 180–340 nm. The mesostructure is similar to that in **Figure 4b** with nanodiscs randomly orientated on the surface of the sphere. When the reaction time is increased, the nanodiscs intended to be

parallel to the sphere surface (**Figure 7**). It is interesting to see that all the nanocrystallites embedded in the nanorods recrystallized into nanocones, which underwent self-orientation into chains to form a radially ordered pattern. Similar mesostructures were also observed by Saito and co-workers, who confirmed that the ZnO spherical particles were made from wedge-shape units radially aligned along the c-axis and the entire particle is terminated by a single c(+)-plane.[22,32] However, the formation mechanism was not discussed in detail.
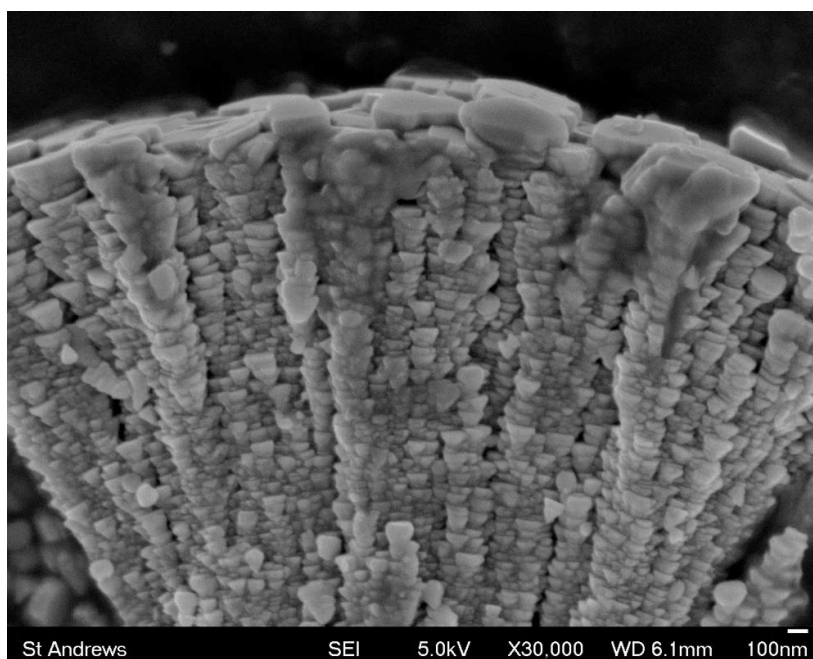

Figure 7. SEM image of a fragment of a spherical particle in the 24 h sample with relatively larger nanodiscs parallel to the surface (top) and all the nanocones in the core lined up in a radial arrangement.

The change in component particles to a pyramidal shape inside the nanorods is believed to occur via further crystal growth in the core and Ostwald ripening through a dissolution–recrystallisation step. A more detailed microstructural evolution is presented by some microscopic images in **ESI,† Figure S9**. With the rapid coalescence of the crystallites, cracks in the spherical particles appeared before they finally broke into wedge-shaped pieces. Comparing the products in the 85%-EG and 95%-EG systems, in particular, noticing that the formation of self-orientated one dimensional nanocone chains only occur in 85%-EG, we can

conclude that water molecules are crucial to the nucleation of ZnO and crystal growth. This has been supported by the isotope tracer study by Saito et al. using $H_2^{18}O$ in the solvent,[32] where ^{18}O transferred from water molecules to the ZnO crystals. The higher concentration of water in the 85%-EG system partially overcame the diffusion problem of water into the spherical particles and enhanced Ostwald ripening in the cores, leading to the formation of nanocones. A similar phenomenon was observed in solvothermal synthesis of perovskite hollow crystals.[33]

Further investigations have been carried out to establish the orientation of the nanocones and how exactly they stack together to form chains. Owing to the already developed surface tiles it seems more plausible that the morphology changes of the building units began at the surface and extended to the core rather than the reverse direction or a simultaneous change throughout the particle. This process is controlled by the diffusion of water molecules. In other words, the concentration of water inside the spherical particles is highest at the surface and is gradually reduced towards the centre of a sphere.

TEM images and corresponding SAED patterns have confirmed the profile view (**Figure 8a**) and the view along the apex (**Figure 8b**) of the nanocones are along the [10$\bar{1}$0] and [0001] zone axes of ZnO. HRTEM images (**Figure 8c** and **ESI,† Figure S10f**) from these view directions show no visible domains and therefore they can be portrayed as a single crystal. Additional SEM and TEM images of nanocones in the 24 h and 48 h specimen are shown in **ESI,† Figure S10(a–e)**. The TEM image in **Figure 8d** shows a chain of nanocones in the 24 h specimen with a dimension in the range of 160–320 nm. The corresponding SAED pattern
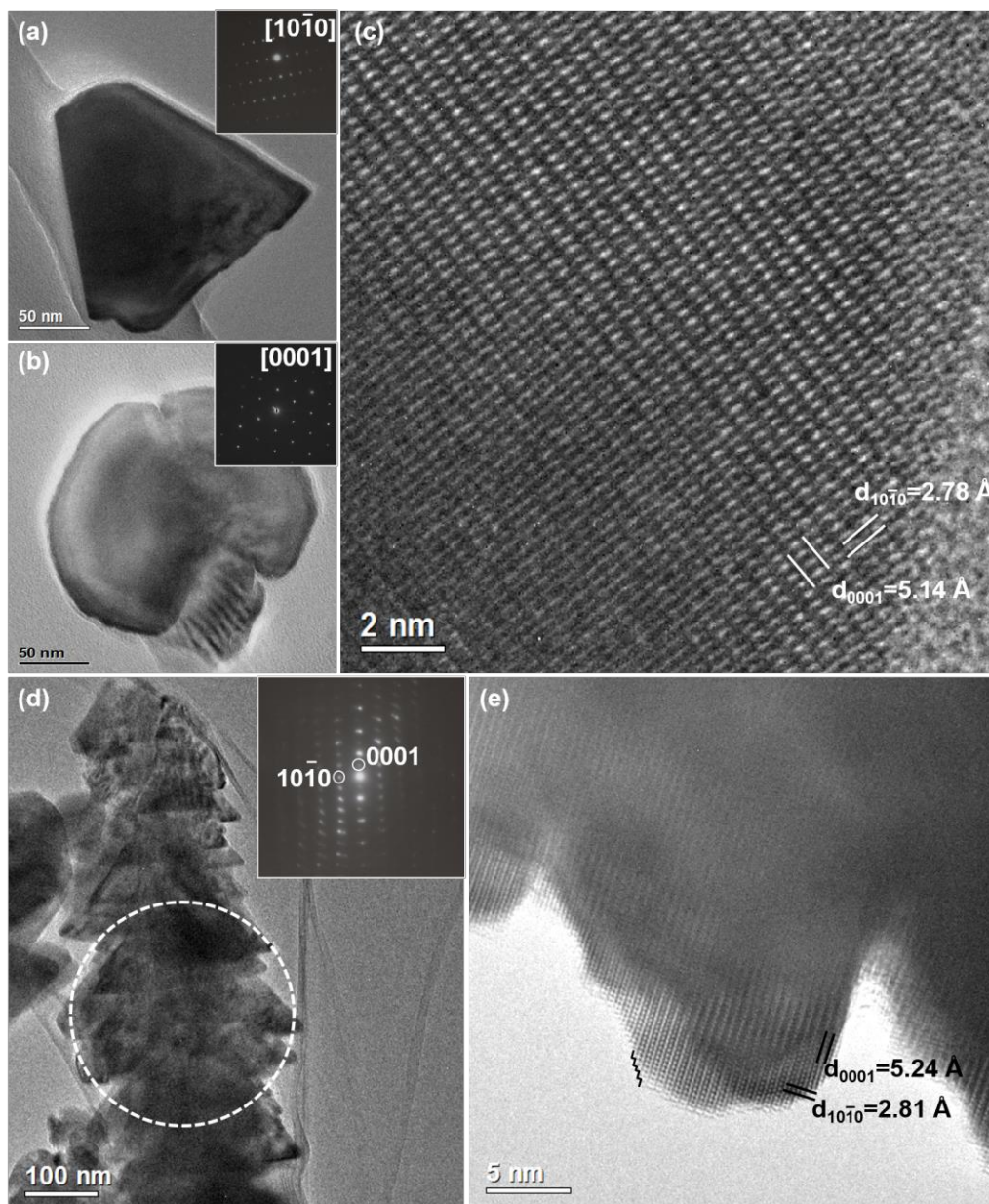
Figure 8. TEM images recorded from specimens prepared in 85%-EG and with a reaction time of 24 h. (a,b) Low magnification TEM image with corresponding SAED pattern (shown in the inset) of nanocones with a view direction of (a) [10$\bar{1}$0] and (b) [0001]. (c) HRTEM image recorded from the nanocone in (a). (d) Low magnification TEM image and corresponding SAED pattern of a chain of nanocones projected along the [01$\bar{1}$0] view direction. (e) HRTEM image showing the uniform orientation of three nanocones aligned in a head-to-tail manner. The side surface of the nanocones are actually formed with nanosteps (marked on HRTEM image) consisting of (0001) and {hk$\overline{h+K}$0} planes.

displayed in the inset shows that a single crystal-like arrangement of diffuse diffraction spots could be obtained when a small selected area aperture is placed into the path of the electron beam. The uniform orientation of nanocones in the chains was further confirmed using

17

HRTEM (**Figure 8e**). Similar TEM and SAED patterns was obtained from a chain of nanocones in the 12 h specimen (**ESI,† Figure S11**). In accordance with the SEM data a smaller particle size of 65–90 nm was observed compared to 160–320 nm for 24 h nanocones. The crystallinity appears to be lower in the 12 h nanocones with the observance of a domain structure as detected during TEM investigations. Secondly, the lattice distortion between the nanocones at 12 h is significantly greater compared to the later reaction times. SAED patterns were recorded from two different locations on the same micro-sized fragment of a spherical particle as further evidence of their c-plane termination (**ESI,† Figure S12**). Although both SAED patterns are projected along the [01$\bar{1}$0] view direction of ZnO, the c-axis has been rotated by 15° indicating the chains of nanocones are radially aligned along the c-axis, which is consistent with literature.[22] Electron microscopic images acquired from a fractured chain of nanocones confirms the surface layer of cones have a significantly larger dimension compared to those located a few layers below (**ESI,† Figure S13a,b**). Similar to the obtained TEM images of the nanocones (**ESI,† Figure S10**), SEM detected several varieties including hollow and solid nanocones. Many nanocones also appeared to be wrapped around the nanocone located underneath (**ESI,† Figure S13c,d**).

ZnO crystals have a typical dipolar structure with a charge separation on the two {0001} surface terminations, i.e. c(+)-plane and c(-)-plane. The formation of nanocones instead of nanorods or hexagonal bifrustum [34] implies that crystal growth only took place on one of the {0001} faces and the growth on the other face, the exposed face on the sphere surface, was suppressed. We assume the exposed faces of nanodiscs on the spherical particles are protected by EG or HMT molecules, these faces more likely terminated with the c(+)-plane. This model agrees with the previous CBED study on ZnO nanocones, in which it was confirmed that the flat base of nanocones, prepared with the same method as that used in this work, terminated at the c(+)-plane.[22,32] The termination plane on the base of the nanocones can be changed to c(-)-plane, if the principal ligands are changed to positively charged molecules. For example,

mixing oleic acid and ethylenediamine to make an ionic solvent, the flat base of ZnO hexagonal micropyramids were terminated by the c(-)-plane.[16]

XPS was used in the present work to determine the terminal atomic layer of the 48 h particles prepared in 95%-EG. The terminal atomic layer of the ZnO particles prepared in 95%-EG has not been reported in literature before. In the present work, the surface of the as-synthesised microspheres were found to be Zn rich with an atomic ratio Zn/O(lattice) of 1.38 (**ESI,† Figure S14**). This result supports our proposed formation mechanism of nanocones.

In both 95%-EG and 85%-EG systems, the nanodiscs developed on the spherical particle surface first. These nanodiscs, with Zn^{2+} terminated outer faces, produced a relatively strong dipolar field, which guided the linear alignment of the smaller nanocrystallites in the cores, no matter if their shape took the form of a sphere, a disc or a cone, to form 1D chains. Ordering of the dipolar fields of the core particles can be also expected. A similar effect of the dipolar field leading to assembly of ZnO nanoparticles into twin polycrystalline particles or mesocrystal microspheres was previously observed.[13,35,36]

2.3. Photodegradation of methylene blue

The photocatalytic decolourisation of MB was carried out with the as-synthesized ZnO spherical samples and compared with ZnO nanorods (**ESI,† Figure S15**) under identical conditions. In addition, the as-synthesized ZnO-48 h spherical sample prepared in 95%-EG solution contains *ca.* 2.1 wt% organics as indicated by the TGA analysis, which could interfere with the photocatalytic activity. The as-synthesized ZnO-48 h sample was calcined under O_2 at 600 ºC for 4 h to remove any organic compounds, prior to examination of the photocatalytic performance. As shown in **Figure 9a**, the initial photocatalytic decolourization rates of all the ZnO samples follow first-order reaction kinetics. The initial degradation rate constant (k, 10^{-3} min^{-1}) could be obtained by plotting Ln(C/C_0) *vs.* Time, where C and C_0 are the concentration at time T and initial concentration. The decolourization rate constants k, are

9.6, 13.0, 17.5, 65.0 for the ZnO-12 h, ZnO-48 h, ZnO-48 h (calcined) and ZnO nanorod samples, respectively. The ZnO spherical sample synthesised with a longer reaction time (48 h) exhibits slightly better performance than the sample prepared in 12 h. Further removal of surface organics of ZnO-48 h by calcination enhanced the photocatalytic activity, but overall the ZnO spherical samples showed much slower decolourisation rates than the ZnO nanorod sample.
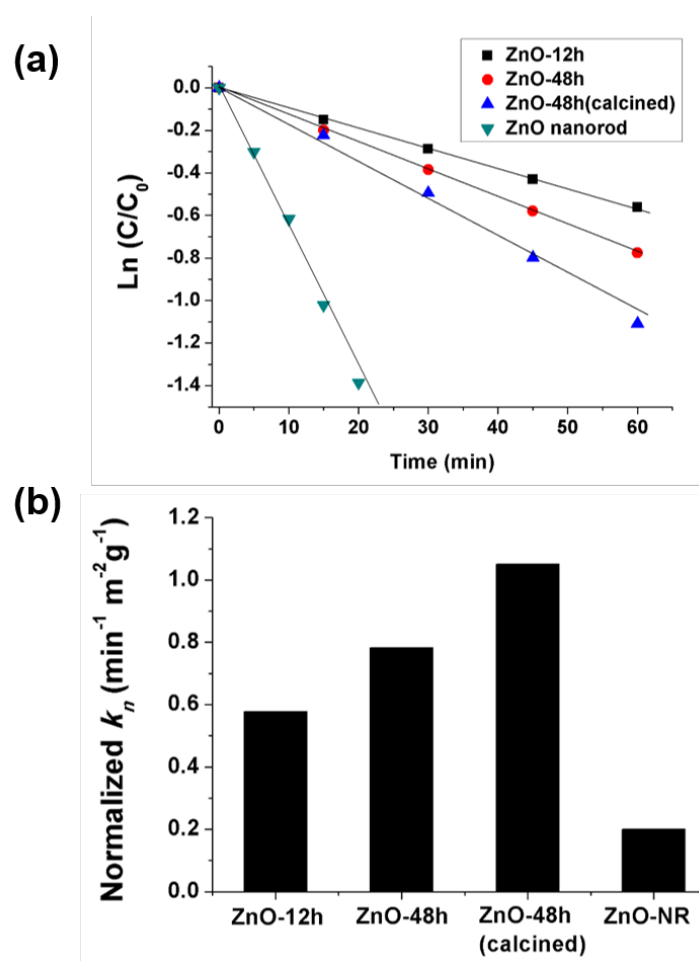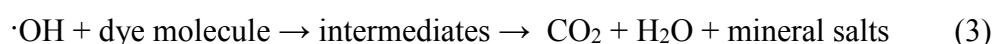

Figure 9. (a) Photocatalytic activities of various ZnO samples for the decolourization of MB dye. (b) Normalized photocatalytic decolourization rate constants k_n, (min^{-1} m^{-2}g^{-1}) of various ZnO samples.

The activity comparison of ZnO spherical samples and ZnO nanorods in terms of the apparent rate constant k, however, is not based on the same surface area of active ZnO component, but on the total mass of the ZnO catalyst. The ZnO spherical samples contain only a small fraction of active surface area (~0.83 m^2/g, mainly as the {0001} exposed surface

layer of nanocones) compared to the ZnO nanorods (~ 16.17 m^2/g) as observed from the SEM images and the BET measurements, the major part of ZnO inside the bulk particles does not participate in the catalytic reaction. Therefore, the photocatalytic decolourization rate constants were normalized by the BET surface area (k_n, min^{-1} $m^{-2}g^{-1}$) and compared as shown in **Figure 9b**. The photocatalytic activities of ZnO spherical samples with exposed {0001} facets are notably higher than the ZnO nanorod sample with most exposed facets being non-polar, implying that the {0001} surface is more photoactive than the other facets for the photocatalytic reaction. The crystallinity effect on the influence of photoactivity is not expected to be dominant, since all the ZnO samples exhibit similar crystallised structure. The {0001} base of the nanocones in the present work is polar and solely terminated by zinc atoms. Preferential adsorption of OH^- ions on this positively charged surface would lead to a higher production of OH• radicals, and therefore faster degradation of the cationic MB dye.[37] Selective deposition of Au nanoparticles on the polar facets of ZnO whilst minimising their distribution on non-polar facets has shown great potential for improving the photocatalytic activity.[38] The photocatalytic degradation of MB can be represented by the follow scheme:

$$ZnO + hv \rightarrow ZnO^* \tag{1}$$

$$ZnO^* + H_2O \rightarrow ZnO^* + H^+ + \cdot OH \tag{2}$$

$$\cdot OH + \text{dye molecule} \rightarrow \text{intermediates} \rightarrow CO_2 + H_2O + \text{mineral salts} \tag{3}$$

2.4. Growth mechanism

Nanotile decorated ZnO microspheres have been fabricated with the surface terminated with the c(+)-plane. The detailed formation mechanism has been proposed based on microstructural studies using electron microscopy as described in **Figure 10**.

No distinct differences were observed during characterisation of the early stage products prepared in 85%-EG and 95%-EG conditions. At the beginning, the precursor molecules/ions aggregated into large spherical particles (**step 1**). Nucleation and crystal growth into ZnO

crystallites, ca. 3–8 nm in diameter, took place in the amorphous matrix (**step 2**). The calculated amount of EG molecules in the 95%-EG particles according to TGA data was 6.9 wt% at 10 h and 2.1 wt% at 48 h. Re-crystallisation occurred to form thin discs on the surface of the microspheres with the exposed surface as the (0001) plane. XPS confirmed the (0001)-plane terminated only by Zn^{2+} is preferentially exposed (**step 3**). Each disc generalised a relatively stronger dipolar field. The nanoparticles initially had a random crystal orientation but with longer thermal treatment times changed to a radial alignment along the c-axis guided by the dipolar field from the surface discs.
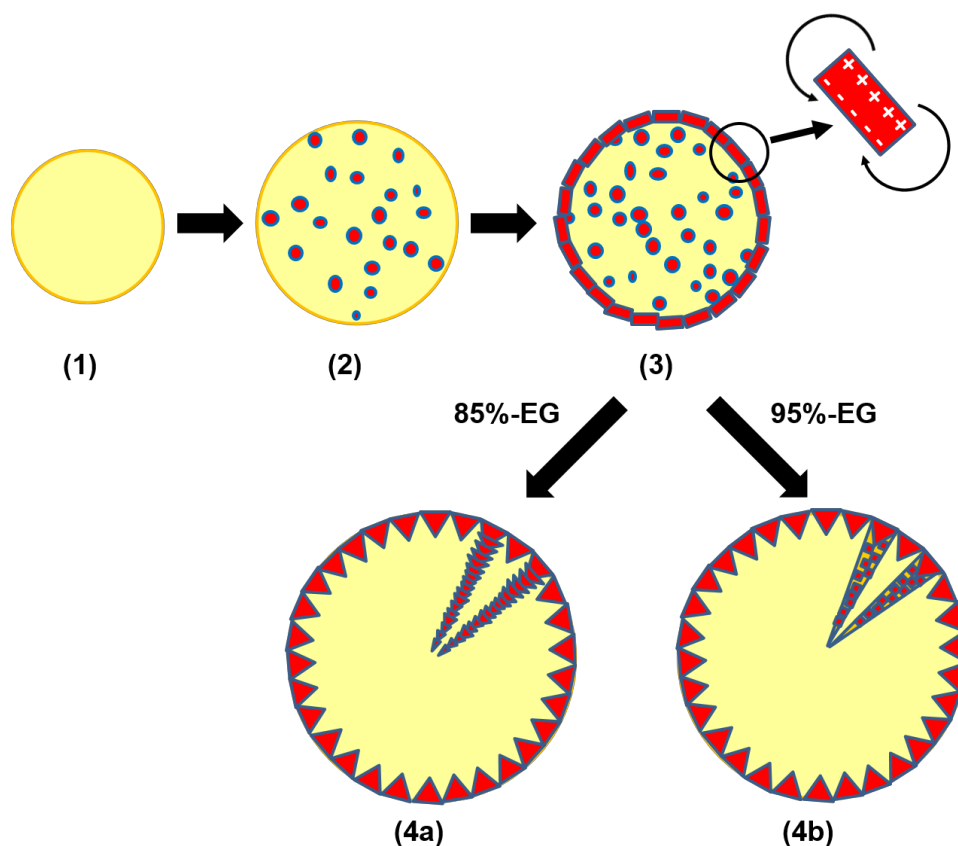

Figure 10. Schematic drawing of the proposed formation mechanism of nanocone decorated ZnO microspheres. Step (1): Aggregation of precursor molecules/ions into large spherical particles. Step (2): Nucleation and growth of ZnO nanocrystallites. Step (3): Surface re-crystallisation into nanodiscs. One nanodisc is enlarged on the right side to show a dipolar field associated with charge separation in the disc. Step (4a): Formation of aligned nanocones in a radial manner in the 85%-EG solution. Step (4b): Formation of a single layer of nanocones with all the nanocrystallites in the core radially aligned in the 95%-EG solution.

Since the Zn^{2+}-terminated surface is protected by ligands, further crystal growth predominately took place on the O^{2-}-terminated surface. Consequently, further crystal growth was inwards to change the surface layer of nanotiles into nanocones. These two nanocone decorated microsphere variants have a dimension of 5 – 12 µm if prepared in 85%-EG and a smaller diameter of 3 – 5 µm if 95%-EG conditions are used. Despite the very similar outer appearance, the microsphere particles prepared in 85%-EG and 95%-EG had very different inner structures, either a radial alignment of nanocones (**step 4a**) or spherical crystallites (**step 4b**). The higher concentration of water molecules in 85%-EG increased the speed of the early stage aggregation and reduced the capping effect of EG sufficiently enough for the component nanocrystallites embedded in the nanorods to undergo dissolution and re-crystallisation into nanocones. These 1D chains of nanocones are perfectly oriented along the c-axis of ZnO with the driving force for such a perfect linear alignment being dipolar field interactions. The side surface of the nanocones did not terminate with the $\{hk\overline{h+k}l\}$ planes, but form small steps consisting of $\{hk\overline{h+k}0\}$ and {0001} planes. It is believed that such a stepped surface was stabilised by surface adsorbed organic ligands. The photocatalytic property was found to vary according to the growth time of the particles. The nanocone decorated microspheres exhibited a slightly better performance than the microspheres containing no surface nanocones or nanodiscs. Additionally, the activity performance of nanocone decorated ZnO microspheres taking into consideration the BET measurements are far superior to ZnO nanorods.

3. Conclusion

In conclusion, ZnO microspheres exposing only the Zn^{2+}-(0001) planes were prepared via a solvothermal route using two different H_2O–EG solvent mixes, 85-vol% and 95 vol%. Electron microscopy revealed their structure, either a core-shell structure containing a single layer of surface nanocones or a 3D radially aligned structure of 1D chains of nanocones whilst

the characterisation of specimens at varying reaction times revealed their formation mechanisms. The significantly improved photocatalytic performance of these ZnO microspheres compared to traditional ZnO nanorods highlights the importance of controlled synthesis of ZnO as well as other transition metal oxide particles with their highly reactive {0001} facets preferentially exposed leading to enhanced photocatalytic, electrochemical and gas sensing performances.

4. Experimental Section

All chemicals were purchased from commercial sources, and were used without further purification, these including $Zn(O_2CCH_3)_2 \cdot 2H_2O$ (ACS grade, from Alfa Aesar), $Zn(NO_3)_2.6H_2O$ (General purpose grade, from Fisher), hexamethylenetetramine (HMT) (Reagent grade, from Sigma Aldrich), ethylene glycol (EG) (Reagent grade, from Fisher).

Preparation of ZnO specimens in 95 vol%-EG (thereafter 95%-EG): The synthetic method for ZnO is a modification of that used by Matsumoto *et al.*[22] $Zn(O_2CCH_3)_2 \cdot 2H_2O$ (2.202 g, 10.03 mmol) and HMT (1.682 g, 12 mmol) were each dissolved in 20 mL of a 95 vol% solution of EG with water. The mixed solution was sealed in a Teflon-lined stainless steel autoclave and heated in an oven at 95 °C for various lengths of time. The resulting precipitate was recovered by centrifugation (at 3400 r.p.m. for 5 min), followed by washing three times with ethanol. The precipitate was then dried at 60 °C overnight. To study the step-by-step growth mechanism, specimens were synthesised under identical conditions except different thermal reaction times of 10 h, 12 h, 18 h, 24 h, 48 h and 96 h were applied.

Preparation of ZnO specimens in 85 vol%-EG (thereafter 85%-EG): $Zn(O_2CCH_3)_2 \cdot 2H_2O$ (2.634 g, 12 mmol) and HMT (1.682 g, 12 mmol) were each dissolved in 20 mL of 85 vol% mixed solvent of EG with water, followed by the same treatments as that for ZnO prepared in 95 vol%-EG. The specimens were recovered after different thermal reaction times of 6 h, 8 h, 10 h, 12 h, 24 h, 48 h and 96 h.

Zinc precursor effect: To study the importance of the zinc precursor, $Zn(NO_3)_2.6H_2O$ was used instead of $Zn(O_2CCH_3)_2\cdot2H_2O$. The synthetic conditions were the same as that for ZnO using $Zn(O_2CCH_3)_2\cdot2H_2O$ as precursor in 95 vol%-EG.

Preparation of ZnO nanorods: The thermal decomposition of $Zn(O_2CCH_3)_2\cdot2H_2O$ (1.46 g) was carried out in a tube furnace under O_2 at 286 °C for 4 h with a ramp rate of 5 °C min^{-1}.

Characterisation: XRD was performed on a PANalytical Empyrean diffractometer, using Cu Kα radiation (λ = 1.5418 Å). Analysis of the powder XRD patterns was carried out using Highscore plus software. SEM images of the specimens were obtained using a JEOL JSM-6700F field-emission gun microscope, operating at 5 kV. To overcome beam charging problems, the specimen surface was coated with a thin gold film using a Quorum Technologies Q150R ES sputter/ carbon coater prior to SEM analysis. The FEG-SEM is equipped with an Oxford INCA system for EDX, which was applied for examination of the local chemical compositions of the specimens. TEM images and SAED patterns were attained using a JEOL JEM-2011 electron microscope fitted with a LaB_6 filament operating at an accelerating voltage of 200 kV. The TEM and HRTEM images were recorded using a Gatan 794 CCD camera. This electron microscope is also equipped with an Oxford Link ISIS SemiSTEM EDX system. TGA was carried out on a Stanton Redcroft STA-780 series instrument at a heating rate of 5°C/min in air. Examination of the porosity, the BET surface area were measured by N_2 adsorption/desorption isotherms at -196 °C on a Micromeritics Tristar II 3020 instrument. XPS was carried out on a Kratos Axis Ultra-DLD photoelectron spectrometer equipped with an Al monochromatic X-ray source. The data were analysed using CasaXPS software. Quantification was carried out on the peaks of interest (Zn 2p3/2, O 1s) using a linear type background subtraction and fitted with individual components.

Photocatalytic degradation of methylene blue: The photocatalytic activities of the ZnO samples were investigated by employing MB dye as a model substrate. An aqueous suspension of ZnO catalyst (20 mg / 20 ml) with 100 μM MB was put in a 25 mL glass vial

reactor. A 250 W iron-doped halide lamp was used as a UV light source. The reactor was open to ambient air. The suspension was stirred for 0.5 h in the dark to allow the adsorption equilibrium of MB on the catalyst. Sample aliquots were withdrawn from the reactor intermittently during the illumination. The concentration of MB dye was determined by measuring the maximum absorbance at 665 nm with a UV-vis spectrophotometer. The photocatalytic activity was quantified in terms of the apparent first-order rate constant (k) for the decolourization of MB under irradiation.

Supporting Information
Supporting Information is available from the Wiley Online Library or from the author.

Received: ((will be filled in by the editorial staff))
Revised: ((will be filled in by the editorial staff))
Published online: ((will be filled in by the editorial staff))

References

[1] H. Wilmer, M. Kurtz, K. V. Klementiev, O. P. Tkachenko, W. Grünert, O. Hinrichsen, A. Birkner, S. Rabe, K. Merz, M. Driess, C. Wöll, M. Muhler, *Phys. Chem. Chem. Phys.* **2003**, 5, 4736.

[2] M. Law, L. E. Greene, J. C. Johnson, R. Saykally, P. Yang, *Nat. Mater.* **2005**, 4, 455.

[3] Y.-S. Choi, J.-W. Kang, D.-K. Hwang, S.-J. Park, *IEEE Trans. Electron Dev.* **2010**, 57, 26.

[4] L. Vayssieres, K. Keis, A. Hagfeldt, S.-E. Lindquist, *Chem. Mater.* **2001**, 13, 4395.

[5] A. Umar, M. M. Rahman, S. H. Kim, Y.-B. Hahn, *Chem. Commun.* **2008**, 166.

[6] R. Shi, P. Yang, J. Wang, A. Zhang, Y. Zhu, Y. Cao, Q. Ma, *CrystEngComm* **2012**, 14, 5996.

[7]   F. Li, Y. Ding, P. X. X. Gao, X. Q. Xin, Z. L. Wang, *Angew. Chem. Int. Ed.* **2004**, 43, 5238.

[8]   Y. K. Mishra, G. Modi, V. Cretu, V. Postica, O. Lupan, T. Reimer, I. Paulowicz, V. Hrkac, W. Benecke, L. Kienle, R. Adelung, *ASC Appl. Mater. Interfaces* **2015**, 7, 14303.

[9]   O. Lupan, L. Chow, G. Chai, H. Heinrich, *Chem. Phys. Lett.* **2008**, 465, 249.

[10]   B. Liu, H. C. Zeng, *J. Am. Chem. Soc.* **2004**, 126, 16744.

[11]   L. Chow, O. Lupan, H. Heinrich, G. Chai, *Appl. Phys. Lett.* **2009**, 94, 163105.

[12]   Y. Sun, L. Wang, X. Yu, K. Chen, *CrystEngComm*, **2012**, 14, 3199.

[13]   H. F. Greer, W. Z. Zhou, M.-H. Liu, Y.-H. Tseng, C.-Y. Mou, *CrystEngComm* **2012**, 14, 1247.

[14]   H. Kaftelen, K. Ocakoglu, R. Thomann, S. Tu, S. Weber, E. Erdem, *Phys. Rev. B* **2012**, 86, 014113.

[15]   B. Ludi, M. Niederberger, *Dalton Trans.* **2013**, 42, 12554.

[16]   X. Zhou, Z.-X. Xie, Z.-Y. Jiang, Q. Kuang, S.-H. Zhang, T. Xu, R.-B. Huang, L.-S. Zheng, *Chem. Commun.* **2005**, 5572.

[17]   N. P. Herring, K. AbouZeid, M. B. Mohamed, J. Pinsk, M. S. El-Shall, *Langmuir* **2011**, 27, 15146.

[18]   S. Hussain, T. Liu, M. Kashif, S. Cao, W. Zeng, S. Xu, K. Naseer, U. Hashim, *Mater. Lett.* **2014**, 128, 35.

[19]   M. Huang, S. Weng, B. Wang, J. Hu, X. Fu, P. Liu, *J. Phys. Chem. C* **2014**, 118, 25434.

[20]   F. Li, F. Gong, Y. Xiao, A. Zhang, A. Zhao, A. Zhao, J. Zhao, S. Fang, D. Jia, *Nano*, **2013**, 23, 10482.

[21]   T. Ihara, H. Wagata, T. Kogure, K.-I. Katsumata, K. Okada, N. Matsushita, *RSC Adv.* **2014**, 4, 25148.

[22]   K. Matsumoto, N. Saito, T. Mitate, J. Hojo, M. Inada, H. Haneda, *Cryst. Growth Des.* **2009**, 9, 5014.

[23]   N. Saito, K. Matsumoto, K. Watanabe, T. Aubert, F. Grasset, I. Sakaguchi, H. Haneda, *J. Ceram. Soc. Jpn.*, **2014**, 122, 488.

[24]   P. Hu, X. Zhang, N. Han, W. Xiang, Y. Cao, F. Yuan, *Cryst. Growth Des.* **2011**, 11, 1520.

[25]   W.-J. Ong, L.-L. Tan, S.-P. Chai, S.-T. Yong, A. R. Mohamed, *Nanoscale*, **2014**, 6, 1946.

[26]   D. Su, X. Xie, S. Dou, G. Wang, *Sci. Rep.*, **2014**, 6, 5753.

[27]   U. K. Gautam, M. Imura, C. S. Rout, Y. Bando, X. Fang, B. Dierre, L. Sakharov, A.wan Govindaraj, T. Sekiguchi, D. Golberg, C. N. R. Rao, *Proc. Natl. Acad. Sci.* **2010**, 107, 13588.

[28]   J. N. van Niekerk, F. R. L. Schoening, J. H. Talbot, *Acta Cryst.*, **1953**, 6, 720.

[29]   X. Y. Chen, M. H. Qiao, S. H. Xie, K. N. Fan, W. Z. Zhou, H. Y. He *J. Am. Chem. Soc.*, **2007**, 129, 13305.

[30]   H. Greer, P. S. Wheatley, S. E. Ashbrook, R. E. Morris, W. Z. Zhou, *J. Am. Chem. Soc.*, **2009**, 131, 17986.

[31]   K. Self, H. Zhou, H. F. Greer, Z. R. Tian, W. Z. Zhou, *Chem. Commun.*, **2013**, 49, 5411.

[32]   N. Saito, K. Matsumoto, K. Watanabe, M. Hashiguchi, I. Sakaguchi, H. Haneda, *Cryst. Growth Des.* **2015**, 15, 2609.

[33]   X. F. Yang, J. X. Fu, C. J. Jin, J. Chen, C. L. Liang, M. M. Wu, W. Z. Zhou, *J. Am. Chem. Soc.*, **2010**, 132, 14279.

[34]   K. He, G. L. Zhao, G. R. Han, *CrystEngComm*, **2014**, 16, 3853.

[35]   M.-H. Liu, Y.-H. Tseng, H. F. Greer, W. Z. Zhou, C.-Y. Mou., *Chem. Eur. J.*, **2012**, 18, 16104.

[36]   Z. Liu, X. D. Wen, X. L. Wu, Y. J. Gao, H. T. Chen, J. Zhu, P. K. Chu, *J. Am. Chem. Soc.*, **2009**, 131, 9405.

[37]   A. Mclaren, T. Valdes-Solis, G. Li, S. C. Tsang, *J. Am. Chem. Soc.*, **2009**, 131, 12540.

[38]   X. Xuewen, W. Wang, Y. Miao, G. Feng, R. Zhang, *J. Colloid Interf. Sci.*, **2016**, 475, 112.